Transactions in GIS, 2002, 6(4): 403–429

Research Article

An Evaluation of Four Different Wavelet Decomposition Procedures for Spatial Feature Discrimination in Urban Areas

Soe Win Myint
Department of Geography
University of Oklahoma

Nina Lam
Department of Geography
Louisiana State University

John Tyler
Department of Computer Science
Louisiana State University

Abstract
Texture or spatial arrangement of neighborhood objects and features plays an important role in the human visual system for pattern recognition and image classification. The traditional spectral-based image processing techniques have proven inadequate for urban land use and land cover mapping from images acquired by the current generation of fine-resolution satellites. This is because of the high frequency spatial arrangements or complex nature of urban features. There is a need for an effective algorithm to digitally classify urban land use and land cover categories using high-resolution image data. Recent studies using wavelet transforms for texture analysis have generally reported better accuracy. Based on a high-resolution ATLAS image, this study illustrates four different wavelet decomposition procedures – the standard, horizontal, vertical, and diagonal decompositions – for urban land use and land cover feature extraction with the use of 33×33 pixel samples. The standard decomposition approach was found to be the most efficient approach in urban texture analysis and classification. For comparison purposes and to better evaluate the accuracy of wavelet approaches in image classification, spatial autocorrelation techniques (Moran's *I* and Geary's *C*) and the spatial co-occurrence matrix method were also examined. The results suggest that the wavelet transform approach is superior to all other approaches.

Address for correspondence: Soe Win Myint, Department of Geography, University of Oklahoma, 100 East Boyd Street, Norman, OK 73019-1007, USA. E-mail: swmyint@ou.edu

1 Introduction

Results obtained from urban land use and land cover mapping generally are much less accurate while applications of remotely sensed image data have been successful in other areas (e.g. agriculture, forestry, wetland, water resources, soil, land, etc.). The traditional spectral-based image processing techniques have proven inadequate, due to the lack of consideration of the spatial properties of images in classifying the urban land-use and land-cover features in high-resolution images. Some researchers may think that high-resolution image data would provide better accuracy in image processing and classification since it contains more detailed information. Others, however, report that finer resolution image data does not necessarily improve traditional spectral based image classification (Martin et al. 1988, Green et al. 1993, Muller 1997). In fact, some studies suggest that a reduction in the classification accuracy occurs with high-resolution images, relative to that obtained using coarser resolution data (Haack et al. 1987, Martin et al. 1988, Barnsley and Barr 1996).

As the spatial resolution of remotely sensed data gets finer, detailed objects and features in urban areas (e.g. single family vs. multi family homes, roads, trees, parking lots, etc.) become more detectable; therefore, the spectral reflectance of an urban environment as a whole becomes more complex. Moreover, urban features are composed of spectrally different diverse materials concentrated in a small area (e.g. plastic, metal, rubber, glass, cement, wood, etc.). In fact, the high frequency spatial appearance or complex nature of urban features may be the major limitation in urban land use and land cover classification using high-resolution image data.

The classification accuracy of images is the result of a trade off between two main factors: class boundary pixels and within-class variances (Fortin 1992, Metzger and Muller 1996). Boundary pixels between classes are generally undesirable for classification purposes, even though they may provide useful information on the structure and diversity of landscapes from an ecotone perspective. The within-class variance is often considered a major criterion of accuracy in image classification. With higher ground resolution, the amount of area occupied by boundary pixels decreases but the within-class variance increases. Other factors limiting the accuracy of a classification result are the low between-class variance and the poor representativity of conventional statistical parameters, such as the mean values and the standard deviations.

Most common image processing algorithms do not take the local structure or the spatial arrangement of neighborhood pixels into consideration in the classification. To extract the heterogeneous nature of urban features in high-resolution images, we need to consider the texture information contained in a group of neighborhood pixels, instead of its individual spectral value. Traditional spectral classification algorithms use individual pixel values and ignore spatial information. This spatial information is crucial in urban land use and land cover mapping, because most of the urban land cover classes contain a number of spectrally different pixels or objects. For example, roads, houses, grasses, trees, bare soil, shrubs, swimming pools and footpaths, each of which may have a completely different spectral response, may need to be considered together as a residential class.

Another problem for supervised classification is that it is extremely difficult to define suitable training sets for many categories within urban environments. This is due

to variation in the spectral response of their component land cover types (Foster 1985, Gong and Howarth 1990, Barnsley et al. 1991). Thus, the training statistics may exhibit very high standard deviation (Sadler et al. 1991) and violate one of the basic assumptions of the widely used maximum-likelihood decision rule, namely, that the pixel values follow a multivariate normal distribution (Barnsley et al. 1991, Sadler et al. 1991). Various attempts, including some new spatial and texture analysis techniques, have been proposed to overcome the limitations associated with urban land use and land cover mapping during the past two decades (Gong and Howarth 1992, Barnsley and Barr 1996, Ji and Jensen 1999). The objective of this paper is to compare the performance of the four different decomposition approaches in wavelet analysis in extracting urban features using a relatively small local window (33x33 pixels). This paper also examines the accuracy associated with separate and combinations of different decomposition levels, different wavelet texture measures, and different remote sensing image bands. Other texture methods including spatial autocorrelation and spatial co-occurrence matrix approaches are also tested and their results are compared with that of the wavelet approach.

2 Texture

Texture plays an important role in the human visual system for pattern recognition and interpretation. In image interpretation, pattern is defined as the overall spatial form of related features, and the repetition of certain forms is a characteristic pattern found in many cultural objects and some natural features. Texture is the visual impression of coarseness or smoothness caused by the variability or uniformity of image tone or color (Avery and Berlin 1992). This general description does not reflect the complete characterization of a texture, but it is by far the most commonly used explanation of texture in image analysis and classification. Texture can be evaluated as being fine, coarse, smooth, rippled, molled, irregular, or lineated. Texture is an innate property of virtually all surfaces (e.g. the grain of wood, the weave of a fabric, the pattern of crops in a field, etc.). It contains important information about the structural arrangement of surfaces and their relationship to the surrounding environment. Although it is quite easy for human observers to recognize and describe in empirical terms, texture has been extremely refractory to precise definition and to analysis by digital computers (Haralick et al. 1973). In general, researchers in image analysis and pattern recognition do not bother to try and define texture precisely. There is no universally accepted mathematical definition of texture.

We show some hypothetical textures to demonstrate the general appearance of textures in a simple manner. A random texture can be observed in Figure 1a. The pixels are uncorrelated. Figure 1b shows a hypothetical deterministic texture (a checkerboard style). It is a strictly ordered pattern, which is fully determined from the knowledge of a small pattern. Observable textures are somewhere between these two extremes. Figures 1c and 1d show examples of random texture (hand-made paper) and a deterministic texture (a brick wall) (Brodatz 1996). Some of the characteristics that may be used to explain texture in different ways may include: (1) irregular and regular, (2) coarse and fine, (3) smooth and rough, (4) orientation, (5) high density and low density, (6) phases, (7) linear and non-linear, and (8) high and low frequency (Figure 2). Since the spatial

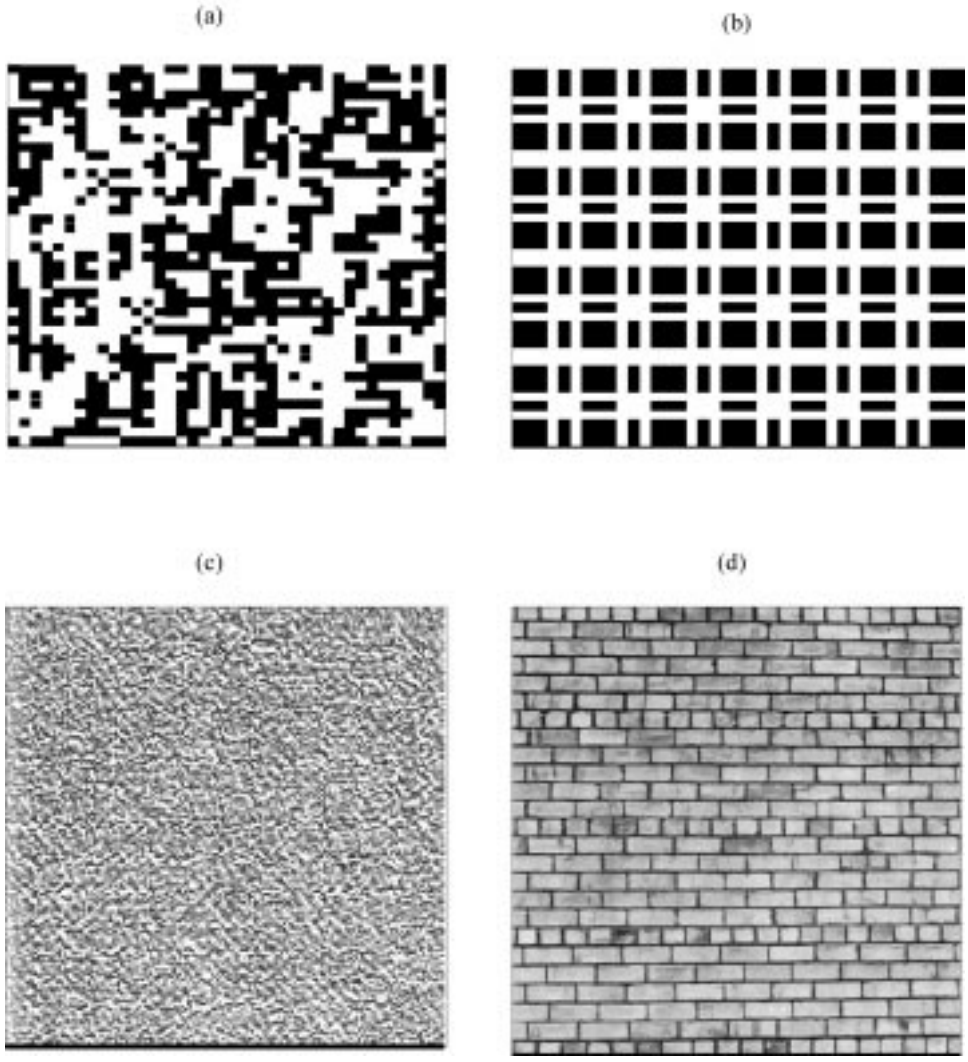

Figure 1 (a) A hypothetical random texture, (b) A hypothetical deterministic texture, (c) Handmade paper (D57 from Brodatz 1966), and (d) Brick wall (D95 from Brodatz 1966)

arrangements of features or textural properties of images appear to carry useful information for discrimination purposes, it is important to develop algorithms and measures to capture the characteristics of texture. Hence, the size of the local window plays an important role in extracting texture information from a given set of data. This is because the minimum distances required to cover different textures may be completely different at a given scale depending on their complexity, repetition, spatial arrangements, orientation, and size of objects and features. This is also true for the same texture features at different scales.

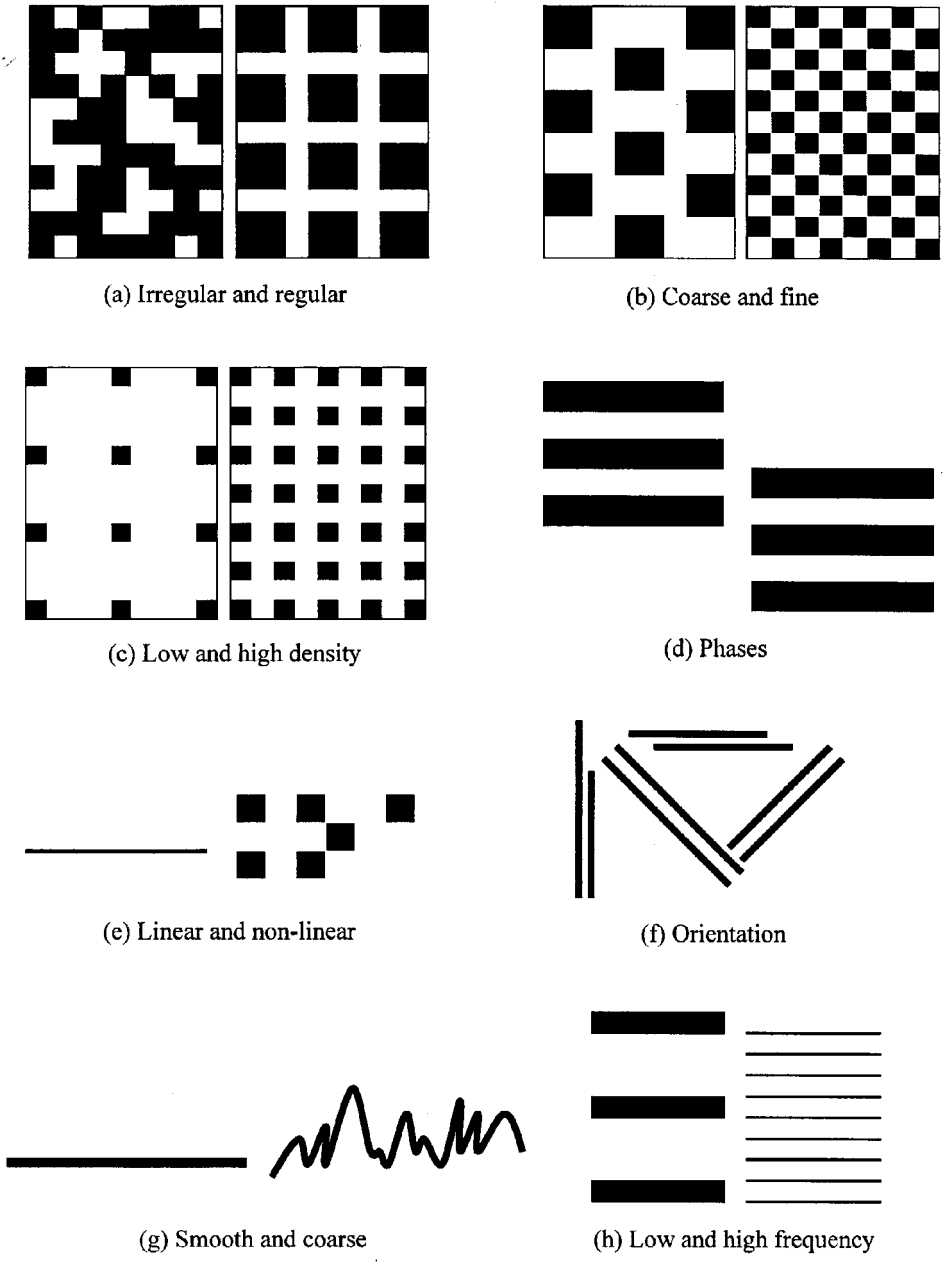

Figure 2 Some characteristics of texture patterns

3 Spatial Analysis and Wavelet Transforms

Local variability in remotely sensed data can be characterized by computing the statistics of a group of pixels, e.g. coefficient of variance or autocovariance, or by analysis of fractal relationships. There have been some attempts to improve the

analysis of remotely sensed data by using texture transforms in which some measure of variability in DN values is estimated within local windows, e.g. contrast between neighboring pixels (Edwards et al. 1988), the standard deviation (Arai 1993), or local variance (Woodcock and Harward 1992). The coefficient of variance gives a measure of the total relative variation of pixel values in an area and can be computed easily, but it provides no information about spatial patterns (De Jong and Burrough 1995). A number of researchers have criticized many other neighborhood operations such as diversity or variation filters (e.g. Klinkenberg 1992, Snow and Mayer 1992, and Burrough 1993). Their results were easy to compare, but they did not reveal any information on spatial irregularities.

De Jong and Burrough (1995) analyzed variograms of remotely sensed measurements to quantitatively describe the spatial patterns. Variogram interpretation of satellite data was also carried out by Woodstock et al. (1988a, b) and Webster et al. (1989). Lam (1990) and Lam and Quattrochi (1992) demonstrated that the fractal dimensions of remote sensing data could yield quantitative insight on the spatial complexity and information content contained within these data. Quattrochi et al. (1997) used a software package known as the Image Characterization and Modeling System (ICAMS) to explore how fractal dimension is related to surface texture. They also investigated how spatial resolution affects the computed fractal dimension of ideal fractal sets by using the isarithm method (Lam and De Cola 1993), the variogram (Mark and Aronson 1984), and the triangular prism methods (Clarke 1986). Emerson et al. (1999) analyzed the fractal dimension using the isarithm method and the spatial autocorrelation methods (Moran's I and Geary's C) to observe the differing spatial structures of the smooth and rough surfaces in remotely sensed images. These approaches, while being applicable, are not problem free. Research on the uses and the limitations of different fractal approaches can be found in Klinkenberg and Goodchild (1992), Xia (1993), Roach and Fung (1994), De Jong and Burrough (1995), Dong (2000a, b), and Lam et al. (2002).

These methods alone may not provide satisfactory accuracy when they are applied to fine-resolution remotely sensed images for urban land cover mapping. Recent developments in the mathematical theory of wavelet transform approaches based on multi-channel or multi-resolution analysis has received some recent attention. In this study, as explained in the next section, wavelet transforms are applied to extract textural features of multispectral urban images.

4 Multi-resolution Wavelet Decomposition

Mallat (1989a, b) developed the multiresolution analysis theory using the orthonormal wavelet basis. A wavelet is orthogonal when all of the pairs formed from the basis functions $\psi_{j,k}$ are orthogonal to each other. An orthogonal wavelet which is normalized to one is called an orthonormal wavelet (Fukuda and Hirosawa 1998). The multiresolution wavelet transform decomposes a signal into a low frequency approximation and high frequency detail information at a coarser resolution. In satellite image analysis using 2-D wavelet transform techniques, rows and columns of image pixels are considered signals.

The approximation and details of a two-dimensional image $f(x,y)$ at resolution 2^j can be defined by the coefficients computed by the following convolutions:

$$A_{2^j}^d f = ((f(x,y)^* \phi_{2^j}(-x)\phi_{2^j}(-y))(2^{-j}n, 2^{-j}m))_{(n,m)\epsilon Z^2} \quad (1)$$

$$D_{2^j}^1 f = ((f(x,y)^* \phi_{2^j}(-x)\psi_{2^j}(-y))(2^{-j}n, 2^{-j}m))_{(n,m)\epsilon Z^2} \quad (2)$$

$$D_{2^j}^1 f = ((f(x,y)^* \psi_{2^j}(-x)\phi_{2^j}(-y))(2^{-j}n, 2^{-j}m))_{(n,m)\epsilon Z^2} \quad (3)$$

$$D_{2^j}^3 f = ((f(x,y)^* \psi_{2^j}(-x)\psi_{2^j}(-y))(2^{-j}n, 2^{-j}m))_{(n,m)\epsilon Z^2} \quad (4)$$

where integer j is a decomposition level, m, n are integers, $\phi(x)$ is a one-dimensional scaling function, and $\psi(x)$ is a one-dimensional wavelet function. In general, $\phi(x)$ is a smoothing function which provides low frequency information (low-pass filter), and $\psi(x)$ is a differencing function which provides high frequency information (high-pass filter). $A_{2^{j+1}}^d f$ can be perfectly reconstructed from $A_{2^j}^d f$, $D_{2^j}^1 f$, $D_{2^j}^2 f$, $D_{2^j}^3 f$.

The expressions (1) through (4) show that in two dimensions, are $A_{2^j}^d f$ and $D_{2^j}^k f$ computed with separable filtering of the signal along the abscissa and ordinate. The wavelet decomposition can thus be interpreted as a signal decomposition in a set of independent, spatially oriented frequency channels (Mallat 1989a), so that $\phi(x)$ and $\psi(x)$ can be defined as:

$$\text{Dilation equation } \phi(t) = \sqrt{2}\sum_k c(k)\phi(2t-k) \quad (5)$$

$$\text{Wavelet equation } \phi(t) = \sqrt{2}\sum_k d(k)\phi(2t-k) \quad (6)$$

For example, Haar, the simplest wavelet transform, has coefficients: $c(0) = c(1) = 1/\sqrt{2}$, $d(0) = 1/\sqrt{2}$, and $d(1) = -1/\sqrt{2}$. Thus, its dilation equation and wavelet equation can be expressed as:

$$\phi(t) = \phi(2t) + \phi(2t-1) \quad (7)$$

$$\psi(t) = \phi(2t) - \phi(2t-1) \quad (8)$$

(Strang and Nguyen 1997).

The approximation and detail coefficients can be computed with a pyramid algorithm based on convolutions with the above-mentioned two one-dimensional parameter filters. Approximation of a signal $A_{2^j}^d f$, also known as trend, can be obtained by convolving the input signal $A_{2^{j+1}}^d f$ with the lowpass filter (L). First, the rows of an image are convolved with a one-dimensional L. Next, the filtered signals are down sampled. In the first step, down sampling is performed by keeping one column out of two. Then the resulting signals are convolved with another one-dimensional lowpass filter, retaining every other row. To obtain a horizontal detail image, first the rows of the input image are convolved with a lowpass filter L, and the filtered signals are down sampled by keeping one column out of two, as we do in processing approximation images. However, for the next stage, the columns of the signals are convolved with a highpass filter H, and again every other row is retained. For the vertical details, the original signals are convolved first with a highpass filter H and then with a lowpass filter L, following the above procedure. For the diagonal detail image, the same down sampling procedure is carried out, using two highpass filters consecutively. The algorithm for the application of the filters and down sampling procedure for computing the approximation and detail coefficients is illustrated in Figure 3. It shows in the frequency domain how the image $A_{2^{j+1}}^d f$ is decomposed into

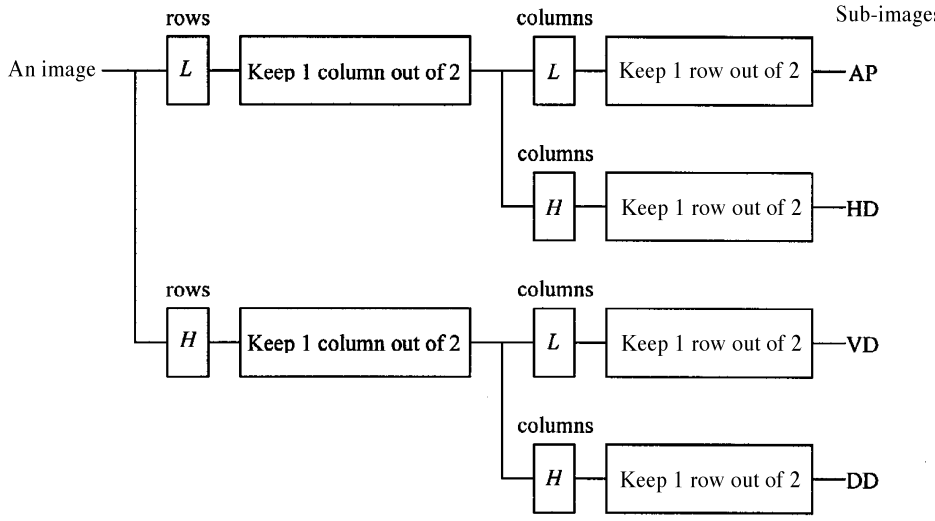

Figure 3 Decomposition procedure of an image by the multiresolution analysis

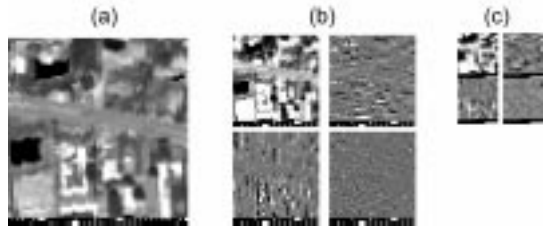

Figure 4 Multiresolution wavelet decomposition of an image (commercial area – near infrared band): (a) original image, (b) wavelet representation at level 1, (c) wavelet representation at level 2

$A^d_{2^j}f$, $D^1_{2^j}f$, $D^2_{2^j}f$, and $D^3_{2^j}f$ sub-images. The sub-image $A^d_{2^j}f$ corresponds to the lowest frequencies (approximation), $D^1_{2^j}f$ gives the vertical high frequencies (horizontal edges), $D^2_{2^j}f$ the horizontal high frequencies (vertical edges), and $D^3_{2^j}f$ the high frequency in both directions (the diagonal edges). Figure 4 represents a standard

orthonormal wavelet decomposition with two levels of an image. The image is a randomly selected training sample of a commercial area generated from the ATLAS image of Baton Rouge, the study area. The pyramid decomposition can be continuously applied to the approximation image until the desired coarseness resolution $2^{-j}(-1 \geq j \geq -J)$ is reached.

5 Data and Study Area

An advanced Thermal Land Application Sensor (ATLAS) image at 2.5 m spatial resolution acquired with 15 channels (0.45 μm−12.2 μm) was used for this study. The data was collected by a NASA Stennis LearJet 23 flying at 6600 feet over Baton Rouge, Louisiana, on May 7 1999 (Figure 5). A previous study by Myint (2001) demonstrated the potential of the wavelet transform approach in texture analysis and classification using 65×65 pixel samples. In this study, we explore further the performance of various wavelet decomposition approaches in classifying urban features with a smaller window (33×33 pixels), and then compare the classification accuracy with that of other texture approaches (spatial autocorrelation and spatial co-occurrence).

Six urban land use and land cover features with different textural appearances were selected. The selected land-use and land-cover classes include single-family homes with less than 50% tree canopy (residential-1), single-family homes with more than 50% tree canopy (residential-2), commercial, forest, agriculture, and water (Figure 6). Two segmented regions of each class were visually identified with the help of local area knowledge, ground information collection, and existing maps. Five training pixels were then randomly selected from each region leading to a sample of 10 pixels. Unlike the 65×65 pixel local window used in the previous study, a 33×33 square window size centered at the randomly selected pixels in each region was used to subset training samples. Criteria for the selection of window size include image resolution, minimum mapping unit size, and the nature of the classes (i.e. minimum distance to completely cover a class, repetition of spatial objects and features of a class, size of the regions, classes selected, level of heterogeneity, and orientation of features) to be identified. The reason for selecting a relatively small window is to see how different wavelet decomposition procedures perform with smaller window sizes. It is understood that a 33×33 pixel local window is large enough to cover texture features of all selected land cover types in this study. In other words, a distance of 33 pixels, 82.5 m in this instance, exceeds the minimum distance required to cover individual texture features of land use and land cover classes in urban areas. It should be noted that small window size may not cover sufficient spatial/texture information to characterize land use and land cover types. At the same time, if the window size is too large, too much information from other land use and land cover features could be included and hence the discrimination result might not be accurate. Therefore, it is important to examine the appropriate window size for accurate discrimination of urban features.

It was observed that textures of the same area in different bands (e.g. visible, reflected infrared, and thermal infrared) were different in terms of contrast, smoothness and coarseness, and spatial variation. Since different texture appearances of the same area in different bands were observed, three different bands were selected and examined in this study. Band-2 (0.52 μm−0.60 μm) was selected as it represents a

Figure 5 A subset of Baton Rouge area displayed in Band-12 (Thermal band—9.60 μm—10.20 μm)

visible band. Band-6 (0.76 μm—0.90 μm) was selected to represent a near infrared band, and band-12 (9.60 μm—10.20 μm) represents a thermal band. Figure 7 shows the differences in texture features of the same area in three different bands: band-2, band-6, and band-12.

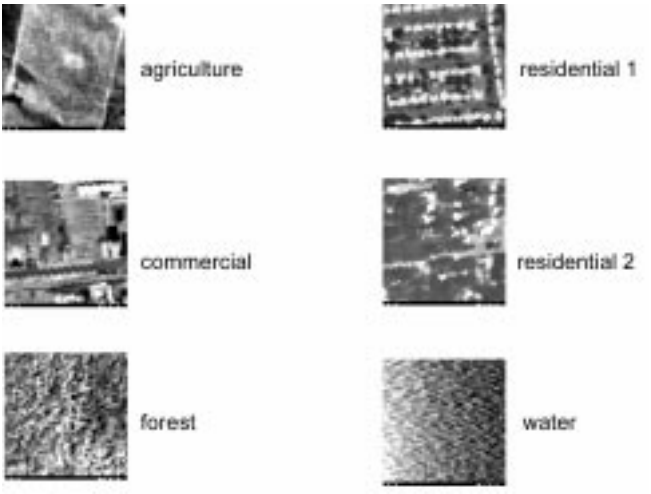

Figure 6 Samples of six urban texture features (Thermal band—9.60 μm—10.20 μm)

Figure 7 Different texture appearances of a sample (commercial) shown in each of the three selected channels: Band-2 (0.52 μm—0.60 μm), Band-6 (0.76 μm—0.90 μm), and band-12 (9.60 μm—10.20 μm).

6 The Analysis Procedure

6.1 Wavelet Transform

Four decomposition approaches were examined in this study: (1) standard decomposition; (2) decomposition with the horizontal details; (3) decomposition with the vertical details; and (4) decomposition with the diagonal details. Figure 8a illustrates the first level decomposition of an original image and Figures 8b-e represent four different decomposition procedures with three levels of an original image. The second, third, and fourth approaches will be hereafter referred to as horizontal decomposition, vertical decomposition, and diagonal decomposition approaches, respectively. These three approaches together are hereafter called detail decomposition techniques. The standard decomposition procedure was carried out for six land cover types of 33×33 pixel texture samples generated from band-2, band-6, and band-12. Then, band-6 samples were further tested with the use of four different decomposition approaches, because band-6 provided the highest accuracy (100%) in the previous study that used 65×65 pixel samples (Myint 2002). To evaluate the power of the wavelet transform technique for texture classification, linear discriminant analysis

approach was used. The texture measures (e.g. entropy value of the decomposed sub-images) for the samples were subject to discriminant analysis. The Minitab software package was used to perform discriminant analysis for the classification of land cover features in this study. The procedure generates a discriminant function (or, for more than two groups, a set of discriminant functions) based on linear combinations of the predictor variables, which provide the best discrimination between the groups. The discriminant analysis was carried out to discriminate between textural features of urban land use and land cover classes on the basis of the texture measure values of the wavelet coefficients of sub-images at different levels.

6.2 *Texture Measures Used to Discriminate Wavelet Features*

Haralick et al. (1973) proposed a variety of measures to extract textural information from the gray level co-occurrence matrices (GLCM), also known as the spatial co-occurrence matrix. Gong and Howarth (1992) demonstrated the efficiency of occurrence frequency methods with the use of several measures: mean, standard deviation, skewness, kurtosis, range, and entropy measures. Zhu and Yang (1998) used information entropy as a measure to identify texture features in 25 types of aerial relief samples selected from remote sensing images. Albuz et al. (1999) used the sum of squares of the wavelet coefficients of each sub-band for their image retrieval system. Sheikholeslami et al. (1999) calculated the mean and variance of wavelet coefficients to represent the contrast of the image. In this study, four feature measures: log energy (*LOG*), Shannon's index (*SHAN*), entropy (*ENT*), and angular second moment (*ASM*) were used to characterize the texture of urban land use and land cover classes:

$$LOG = \sum_{i=1}^{K}\sum_{j=1}^{K} \log(P(i,j)^2) \tag{9}$$

$$SHAN = -\sum_{i=1}^{K}\sum_{j=1}^{K} P(i,j)^{*}\log(P(i,j)) \tag{10}$$

$$ASM = \sum_{i=1}^{K}\sum_{j=1}^{K} p(i,j)^2 \tag{11}$$

$$ENT = -\sum_{i=1}^{K}\sum_{j=1}^{K} Q(i,j)^{*}\log|\,Q(i,j)\,|\,; \quad Q(i,j) = \frac{|P(i,j)|^2}{\sqrt{\sum_{i,j}|P(i,j)|^2}} \tag{12}$$

where $P(i,j)$ is the (i,j)th pixel wavelet coefficient value of a decomposed image at a particular level. A program using the MATLAB software package was developed to perform wavelet decompositions and to compute these four texture measures in the analysis.

6.3 *Other Spatial Approaches*

For comparison and to better evaluate the efficiency of wavelet approaches in image classification, two spatial autocorrelation techniques (Moran's *I* and Geary's *C*) and

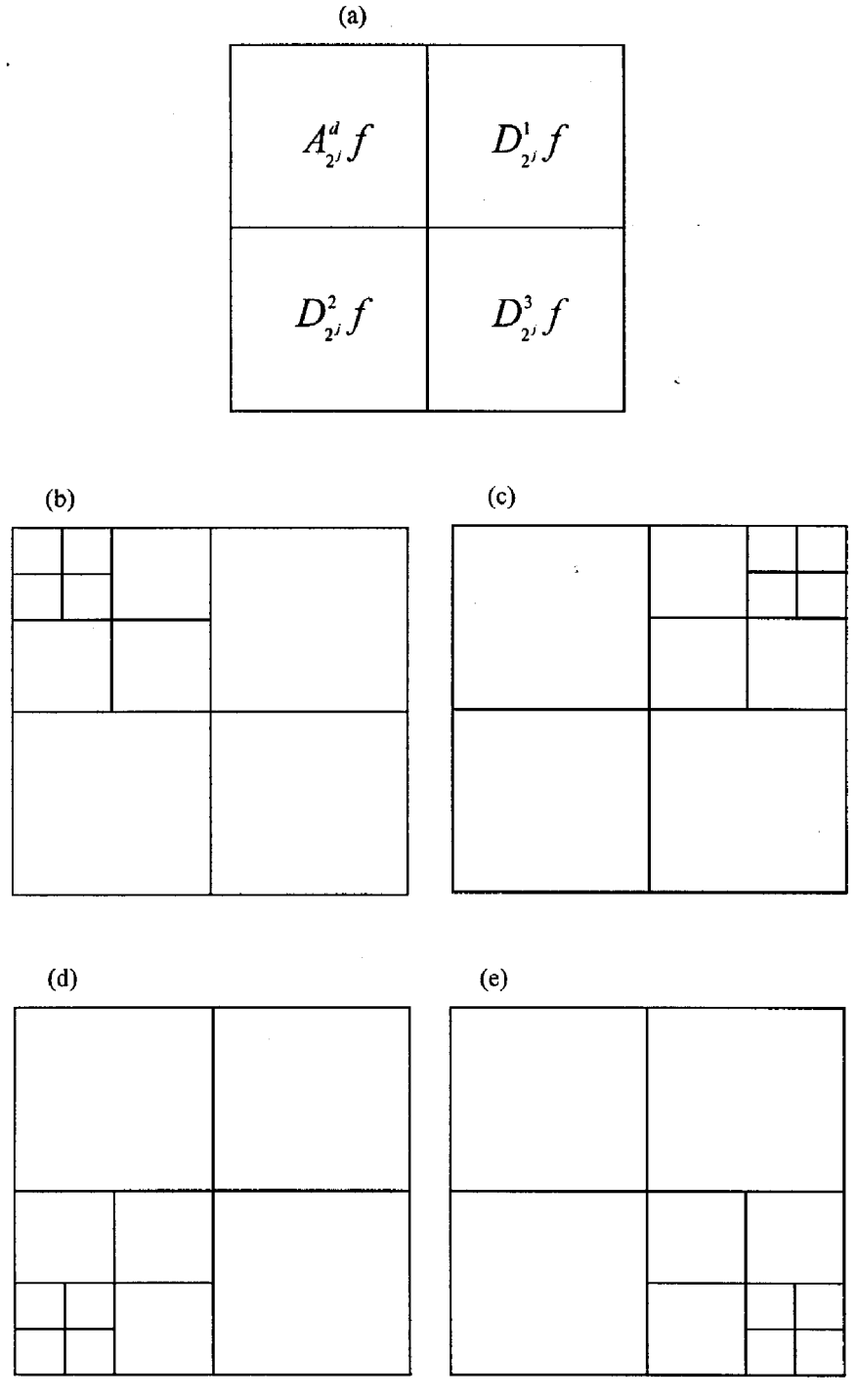

Figure 8 Four different decomposition procedures with 3 levels of an original image; (a) decomposition at the first level, (b) standard, (c) horizontal, (d) vertical, and (e) diagonal decompositions.

the spatial co-occurrence method were also examined in this study. The discriminant analysis was carried out to discriminate between classes of urban land-use and land-cover on the basis of these texture measures.

6.3.1 Spatial Autocorrelation

The software ICAMS was used to compute Moran's *I* and Geary's *C*, the two indices of spatial autocorrelation (Quattrochi et al. 1997, Lam et al. 1998). Moran's *I* and Geary's C are calculated from the following formulae:

$$\mathrm{I}(d) = \frac{n \sum_{i}^{n} \sum_{j}^{n} w_{ij} z_i z_j}{W \sum_{i}^{n} z_i^2} \tag{13}$$

$$\mathrm{C}(d) = \frac{(n-1 \sum_{i}^{n} \sum_{j}^{n} w_{ij} (y_{i-} y_j)^2}{2W \sum_{i}^{n} z_i^2} \tag{14}$$

where w_{ij} is the weight at distance d so that $w_{ij} = 1$ if point j is within distance d from point i; otherwise, $w_{ij} = 0$; z's are deviations (i.e. $z_i = y_i - y_{\text{mean}}$ for variable y), and W is the sum of all the weights where $i \neq j$. Moran's *I* varies from $+1.0$ for perfect positive correlation (a clumped pattern) to -1.0 for perfect negative correlation (checkerboard pattern). Geary's *C* normally ranges from 0.0 to 3.0, with 0.0 indicating positive correlation, 1.0 indicating no correlation, and values greater than 1.0 indicating negative correlation.

6.3.2 Spatial Co-occurrence Matrix

One commonly applied statistical procedure for interpreting texture uses the image spatial co-occurrence matrix (SCM), which is also known as the gray level co-occurrence matrix (GLCM) (Conners and Harlow 1980, Barber and LeDrew 1991, Berry and Goutsias 1991, Pesaresi 2000). The use of SCM or GLCM in texture analysis is also referred to as the spatial gray level dependence method. Spatial co-occurrence matrix is a widely used texture and pattern recognition technique in the analysis of remotely sensed data, and to a certain extent it has been successful.

There are a number of texture measures, which could be applied to spatial co-occurrence matrices for texture analysis. Figure 9 illustrates the construction of four directional spatial co-occurrence matrices for a 3 by 3 window from an example image normalized to four gray levels (0 to 3). The final matrix for a given point location in the image contains the number of times each possible pair of pixel values occurred in the selected orientation (e.g. horizontal 0º, vertical 90º, left diagonal 135º, and right diagonal 45º) within the specified neighborhood surrounding that point (Figure 9c).

In this study, five texture measures based on the co-occurrence matrix were used: angular second moment or Energy (*ASM*); entropy (*ENT*); homogeneity or inverse difference moment (*IDM*), contrast or Inertia (*CON*); and correlation (*COR*). The formulae used to compute each measure from the spatial co-occurrence matrix are as follows (Peddle and Franklin 1991, Conners and Harlow 1980):

(a)

2	0	1
1	2	3
1	1	2

(b)

	0	1	2	3
0	# (0, 0)	# (0, 1)	# (0, 2)	# (0, 3)
1	# (1, 0)	# (1, 1)	# (1, 2)	# (1, 3)
2	# (2, 0)	# (2, 1)	# (2, 2)	# (2, 3)
3	# (3, 0)	# (3, 1)	# (3, 2)	# (3, 3)

(c)

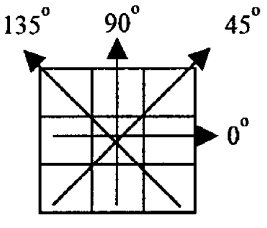

(d)

0	1	1	0
1	2	2	0
1	2	0	1
0	0	1	0

(e)

0	1	0	0
1	0	1	1
0	1	0	0
0	1	0	0

(f)

0	0	1	0
0	2	2	1
1	2	0	1
0	1	1	0

(g)

0	0	0	1
0	1	0	0
0	0	4	0
1	0	0	0

Figure 9 (a) 3×3 window with gray tone range 0—3; (b) General form of any spatial co-occurrence matrix for window with gray tone range 0—3. # (*i,j*) represents number of times gray tones *i* and *j* were neighbors; (c) selected orientations (e.g. horizontal 0º, vertical 90º, left diagonal 135º, and right diagonal 45º); (d)—(f) spatial co-occurrence matrices derived for four angular orientations

$$\text{Angular Second Moment (or) Energy } (ASM) = \sum_i \sum_j p(i,j)^2$$

$$\text{Entropy } (ENT) = \sum_i \sum_j p(i,j)^* \log[p(i,j)]$$

$$\text{Inverse Difference Moment (or) Homogeneity } (IDM) = \sum_i \sum_j \frac{1}{1+(i-j)^2}\, p(i,j)$$

$$\text{Contrast (or) Inertia } (CON) = \sum_i \sum_j (i-j)^2 * p(i,j)$$

where $p(i,j)$ is the (i,j)th pixel co-occurrence matrix value of an image.

7 Results and Discussion

7.1 Standard Decomposition with 33×33 Samples

Using the standard decomposition procedure, linear discriminant analysis was carried out to identify six land cover types of 33×33 pixel texture samples generated from band-2, band-6, and band-12. Wavelet decomposition was performed up to 3 levels, l_1, l_2, and l_3. The classification results are shown in Table 1 and Figure 10.

In the case of band-2, *ENT and ASM* yielded the highest accuracy of 72% at the first decomposition level (Table 1). The overall accuracies produced by *SHAN*, *ENT*, and *ASM* at l_1 and l_2 were slightly higher than those produced by the *LOG* measure. However, there were no significantly different accuracies found between combinations of l_1, l_2, and l_3, (3 levels) and l_1 and l_2 (2 levels). This may be due to the fact that smaller sub-samples at level 3 cover less spatial frequency information. The highest accuracy found in the overall classifications was produced by the combination of 3 levels (90%) when using the *ENT* measure.

In the case of band-6, *ASM* yielded the highest accuracy of 77% at the first level, whereas the *LOG* measure again gave the lowest accuracy (68%) (Table 1). Both *LOG* and *ENT* with the combination of three levels achieved the highest accuracy (88%) in this analysis. Even though the *SHAN* measure yielded the second highest accuracy at the first level it produced the lowest accuracy at the combination of 3 levels (83%).

Table 1 Classification results for bands 2, 6, and 12 using the standard decomposition technique

			Overall Accuracy (%)			
			(Measures)			
Bands	L	NSI	*LOG*	*SHAN*	*ENT*	*ASM*
Band-2 (visible)	l_1	4.0	61.7	70.0	71.7	71.7
	l_2	4.0	40.0	66.7	68.3	70.0
	l_3	4.0	45.0	41.7	48.3	43.3
	$l_1 - l_2$	8.0	73.3	81.7	90.0	83.3
	$l_1 - l_3$	12.0	81.7	83.3	90.0	85.0
Band-6 (near infrared)	l_1	4.0	68.3	75.0	70.0	76.7
	l_2	4.0	53.3	68.3	63.3	68.3
	l_3	4.0	55.0	50.0	56.7	50.0
	$l_1 - l_2$	8.0	78.3	78.3	80.0	76.7
	$l_1 - l_3$	12.0	88.3	83.3	88.3	86.7
Band-12 (thermal)	l_1	4.0	81.7	73.3	80.0	73.3
	l_2	4.0	65.0	65.0	60.0	65.0
	l_3	4.0	45.0	46.7	43.3	46.7
	$l_1 - l_2$	8.0	85.0	90.0	86.7	90.0
	$l_1 - l_3$	12.0	90.0	93.3	90.0	93.3

L = wavelet decomposition level; NSI = number of sub-images

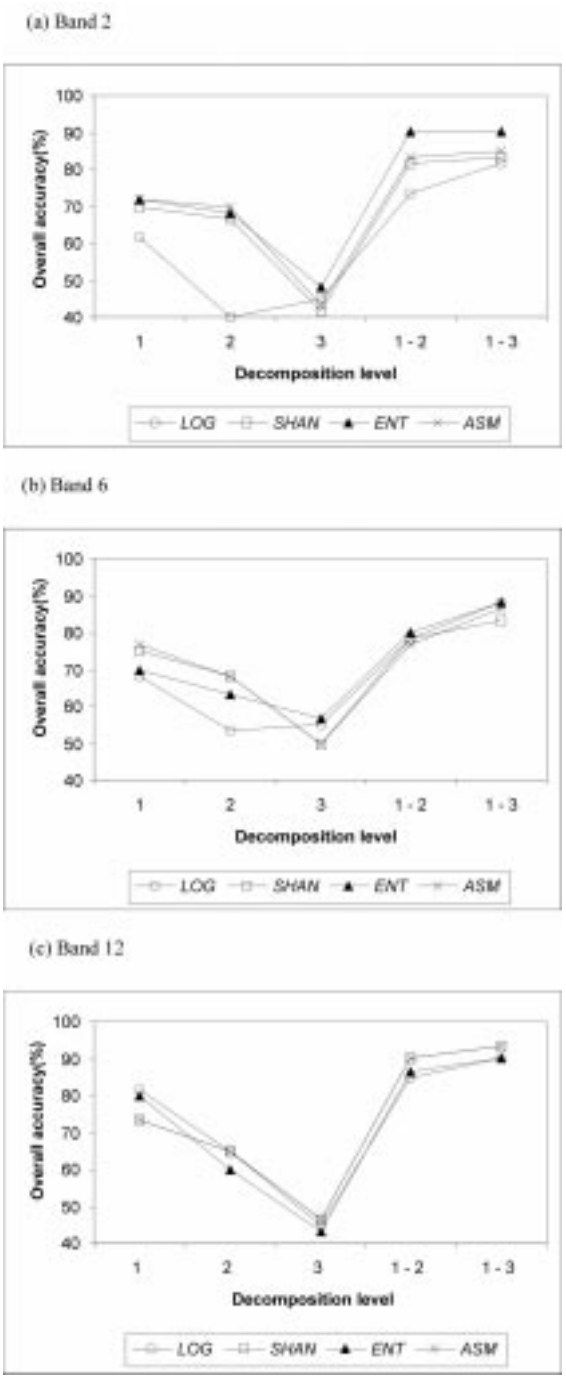

Figure 10 Overall accuracy for *LOG*, *SHAN*, *ENT*, and *ASM* plotted against separate decomposition level and combination of different levels: (a) standard decomposition approach with band 2, (b) standard decomposition approach with band 6, (c) standard decomposition approach with band 12

In the case of band-12, the *LOG* measure yielded the highest accuracy of 82% at the first level. In fact, band-12 with the *LOG* measure gave the highest accuracy among all bands when using level 1 alone. *SHAN* and *ASM* gave the lowest accuracy (73%) at the first level. However, the highest accuracy found in the overall classification was produced by the combination of 3 levels (93%) when using *SHAN* or *ASM* measure.

In general, the range of overall accuracy is relatively large for different measures and for different levels of decomposition. It is observed from Figure 10 that the overall accuracy decreases with increasing decomposition level. This may be due to a reduction in the texture information covered by a smaller image size, since wavelet decomposition at a higher level produces smaller sized sub-images. It is also noted that the accuracy trend curve according to the level of decomposition found in this study is similar to the human detection accuracy curve demonstrated by Hodgson (1998) and the empirical general histogram distance index reported by Pesaresi (2000). Moreover, the overall accuracy for the combination of different levels is much higher than any single level alone. The combination of more levels yielded higher accuracy than that of a lesser number of levels. The highest accuracy found was produced by the combination of l_1, l_2, and l_3. This result was found to be consistent with all measures and all bands.

It is also noted that a measure, which yields the best result at the first level, may not be the most efficient one when using a combination of three levels. In general, the higher the accuracy produced at the first level, the higher the accuracy can be expected when using a combination of three levels for a particular measure. The findings here show that we need to investigate the performance of texture measures using the combination of all levels, regardless of the accuracy achieved at the first level. The reason for this is that the combination of different levels always generates higher accuracy than single levels.

The highest accuracy (93%) found in the classification of 33×33 pixel samples for all three bands was produced by the urban texture features associated with band-12. In general, it can be concluded that band-12 was found to be the most efficient band in this study. The highest overall classification accuracies reported in these analyses with the 33×33 pixel samples generated from band-2, band-6, and band-12 using a combination of all three levels were 90%, 88%, and 93%, respectively (Table 1). The *LOG* measure was generally slightly less accurate than other measures. However, this does not necessarily mean that the *LOG* measure is not a good candidate in texture analysis and classification, since its accuracy exceeded the minimum mapping accuracy of 85% required for most resource management applications when using band-6 and band-12 (Townshend 1981).

It was originally thought that *ENT* would characterize the textures of urban areas more accurately than the others. What has been observed is that other texture measures, in certain situations, produce slightly higher accuracy than the *ENT* measure. However, it is important to note that there is no significant difference in accuracies among all measures. When comparing between bands, samples generated from band-2 produced the lowest accuracies, and band-12 yielded the highest. When all three levels were used, the accuracy level exceeds 85%. Since band-6 was tested in the previous study, we use band-6 to further test the performance of different decomposition approaches and other texture analysis approaches. Finally, when comparing the results among different land cover classes, it is difficult to determine which measure is the most reliable, since both the user's and producer's accuracies for

all classes vary with the use of measure, level of decomposition, and the combination of different levels (Table 2). In general, water may be the most reliable category, which consistently gave relatively high accuracy. This may be because water is more homogeneous in texture than other categories.

7.2 Comparison with Other Decomposition Approaches

In horizontal decomposition, the highest overall classification accuracy (87%) reported in these analyses was produced by the combination of three levels with the use of the *LOG* measure, a value slightly less than that of the standard decomposition approach (Table 3). For other measures, accuracies are significantly lower in horizontal decomposition. This finding is not consistent with the remote sensing image texture analysis reported by Zhu and Yang (1998), where they found the accuracy obtained by horizontal decomposition was slightly superior to the standard decomposition procedure. The discrepancies in results between the two studies might be due to a number of factors, such as local window size, resolution of the image data, nature of the study area, and classification specificity. From Figure 11, we can see the same trend in overall accuracy as we have seen in standard decomposition. It is again observed that sub-images at higher decomposition level produce lower accuracy, and combination of three levels produced the highest accuracy.

In vertical decomposition, the *SHAN* measure with the combination of three levels gave the highest accuracy (87%) (Table 3). The highest overall classification accuracy obtained in this analysis is also lower than the highest accuracy obtained in the standard technique, therefore it can be concluded that vertical decomposition in this study is not as accurate as the standard approach. In addition, the accuracies produced by the vertical approach with the combination of three levels in some cases (e.g. *SHAN*, *ENT*, *ASM*) are higher than the horizontal approach.

In diagonal decomposition, the *LOG* and *ENT* measures with the combination of three levels produced the highest overall classification accuracy (80%) (Table 3). The highest overall classification accuracy obtained in this analysis is lower than the highest accuracy obtained in all other decomposition techniques. It is interesting to note that combination of three levels with the *SHAN* measure produces lower accuracy than the combination of two levels. The lower accuracy of diagonal decomposition may be due to the weaknesses of spatial frequency information captured from diagonal details of the mother body.

The above analysis of different decomposition approaches suggests that the standard approach is generally more accurate than the horizontal, vertical, and diagonal decompositions (Figure 12).

7.3 Comparison with Spatial Autocorrelation and Spatial Co-occurrence Matrix Approaches

Figure 13 and Table 4 present the overall classification accuracies for 33×33 pixel samples produced by wavelet transforms using log energy (W-LOG), Shannon's index (W-SHAN), entropy (W-ENT), and angular second moment (W-ASM); spatial autocorrelation using Moran's I and Geary's C and the spatial co-occurrence matrix

Table 2 Overall classification accuracy and producer's/user's accuracies of the six land-use land-cover classes derived from 33×33 samples of band-6 data

Level	CL	Texture Measures											
		LOG			SHAN			ENT			ASM		
		P_{ACC} (%)	U_{ACC} (%)	O_{ACC} (%)	P_{ACC} (%)	U_{ACC} (%)	O_{ACC} (%)	P_{ACC} (%)	U_{ACC} (%)	O_{ACC} (%)	P_{ACC} (%)	U_{ACC} (%)	O_{ACC} (%)
	A	50	71		40	67		50	50		50	71	
	C	60	67		80	53		50	71		80	57	
	F	70	78		80	100		80	89		80	100	
l_1	L	50	50		60	86		60	75		60	86	
	M	80	73		90	69		90	56		90	69	
	W	100	71		100	91		90	90		100	91	
				68			75			70			76.7
	A	20	33		50	71		60	75		50	71	
	C	50	56		90	69		70	70		90	69	
	F	60	60		80	67		70	64		80	67	
l_2	L	80	67		50	71		40	44		50	71	
	M	60	46		60	50		50	42		60	50	
	W	50	50		80	89		90	90		80	89	
				53			68			63			68.3
	A	40	57		70	64		70	78		60	60	
	C	40	44		40	50		70	70		40	57	
	F	40	40		10	25		10	50		10	20	
l_3	L	60	55		30	30		30	30		30	30	
	M	70	54		60	46		60	43		70	50	
	W	80	80		90	64		100	67		90	64	
				55			50			57			50
	A	80	89		50	83		70	88		60	86	
	C	70	78		90	75		90	90		90	75	
	F	100	100		90	90		90	90		90	100	
$l_1 l_2$ & l_3	L	90	90		90	82		90	90		90	90	
	M	90	90		80	80		90	82		90	82	
	W	100	100		100	91		100	91		100	91	
				88			83			88			86.7

CL = classes; A = agriculture; C = commercial; F = forest; L = single-family homes with less than 50% tree canopy (residential-1); M = single-family homes with more than 50% tree canopy (residential-2); W = water

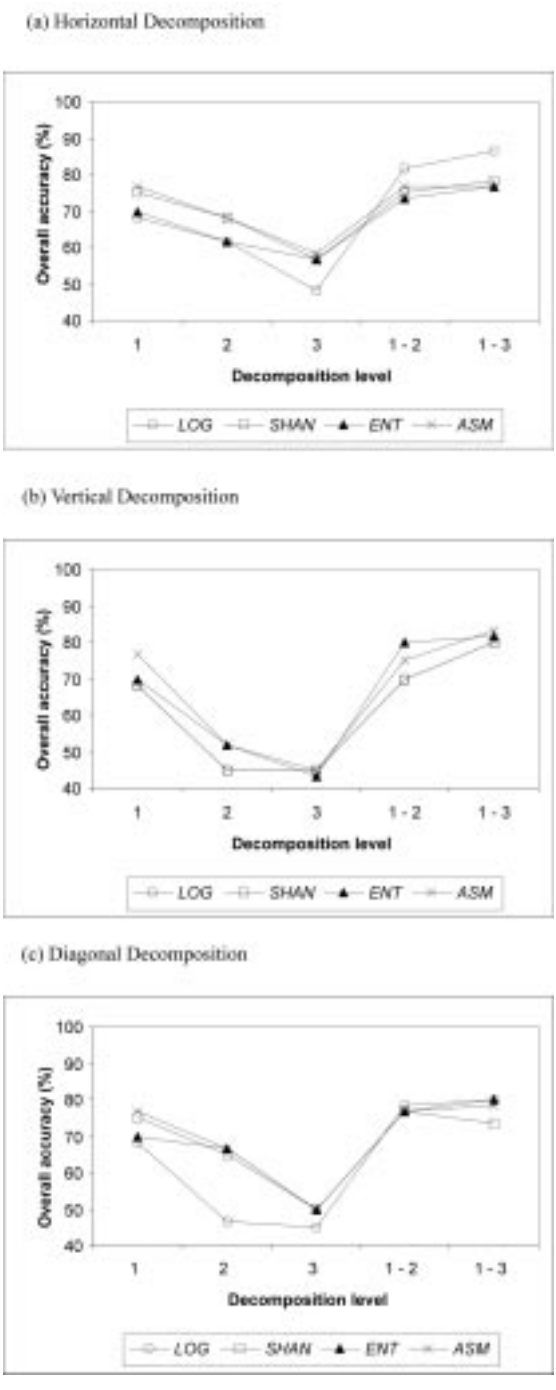

Figure 11 Overall accuracy for *LOG*, *SHAN*, *ENT*, and *ASM* plotted against separate decomposition level and combination of different levels: (a) horizontal decomposition approach with band-6 (33×33), (b) vertical decomposition approach with band-6 (33×33), (c) diagonal decomposition approach for band-6 (33×33)

Table 3 Classification of 33×33 samples generated from band-6 using different decomposition approaches

			Overall Accuracy (%)			
			(Measures)			
Bands	L	NSI	*LOG*	*SHAN*	*ENT*	*ASM*
D1	l_1	4	68.3	75.0	70.0	76.7
	l_2	4	53.3	68.3	63.3	68.3
	l_3	4	55.0	50.0	56.7	50.0
	$l_1 - l_2$	8	78.3	78.3	80.0	76.7
	$l_1 - l_3$	12	88.3	83.3	88.3	86.7
D2	l_1	4	68.3	75.0	70.0	76.7
	l_2	4	61.7	68.3	61.7	68.3
	l_3	4	48.3	56.7	56.7	58.3
	$l_1 - l_2$	8	81.7	75.0	73.3	76.7
	$l_1 - l_3$	12	86.7	78.3	76.7	76.7
D3	l_1	4	68.3	75.0	70.0	76.7
	l_2	4	45.0	51.7	51.7	51.7
	l_3	4	45.0	43.3	43.3	45.0
	$l_1 - l_2$	8	70.0	75.0	80.0	75.0
	$l_1 - l_3$	12	80.0	86.7	81.7	83.3
D4	l_1	4	68.3	75.0	70.0	76.7
	l_2	4	46.7	65.0	66.7	66.7
	l_3	4	45.0	50.0	50.0	50.0
	$l_1 - l_2$	8	78.3	76.7	76.7	76.7
	$l_1 - l_3$	12	80.0	73.3	80.0	78.3

D1 = standard decomposition; D2 = horizontal decomposition, D3 = vertical decomposition; D4 = diagonal decomposition; L = wavelet decomposition level; NSI = number of sub-images

using angular second moment or energy (C-ASM), entropy (C-ENT), homogeneity or inverse difference moment (C-IDM), contrast or inertia (C-CON), and correlation (C-COR).

From Figure 13, it can be noted that the wavelet analysis technique produced more accurate results than other spatial techniques, and the spatial co-occurrence technique yields the lowest accuracy. A standard decomposition approach with three levels combined yielded over 83% accuracies (Table 4). The next highest accuracy is achieved by the spatial co-occurrence matrix with the IDM measure (67%). It is noted that there is a huge gap between the lowest accuracy (83%) achieved by wavelet and the lowest accuracies (60% and 52%) achieved by the other texture methods (i.e. the spatial autocorrelation and spatial co-occurrence matrix approaches). In general, the highest accuracies for the 33×33 pixel samples produced by different texture methods: wavelet transform, spatial autocorrelation, and spatial co-occurrence approaches are 88%, 62%, and 67%, respectively. It is hard to conclude which approach is more accurate

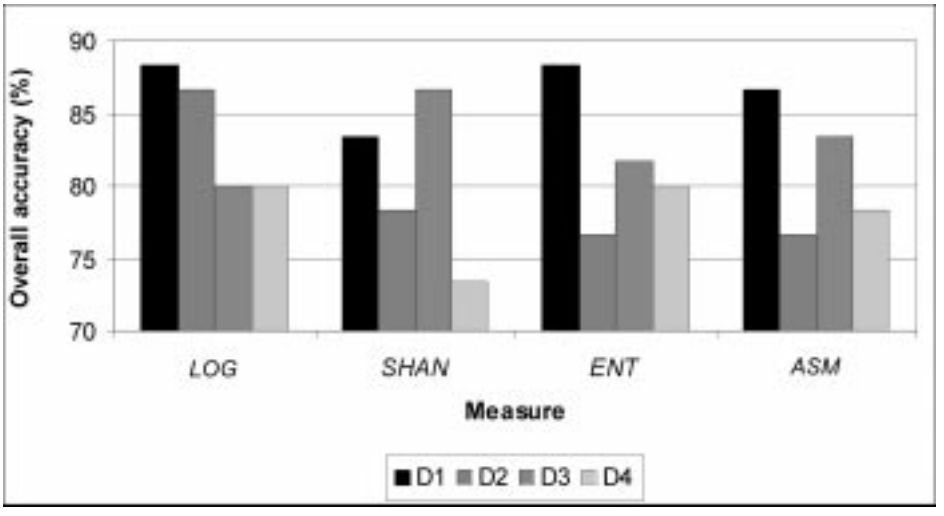

Figure 12 Comparisons of overall accuracies obtained from four different decomposition approaches with band-6 (33×33) using combination of 3 levels: D1 = standard decomposition; D2 = horizontal decomposition, D3 = vertical decomposition; D4 = diagonal decomposition

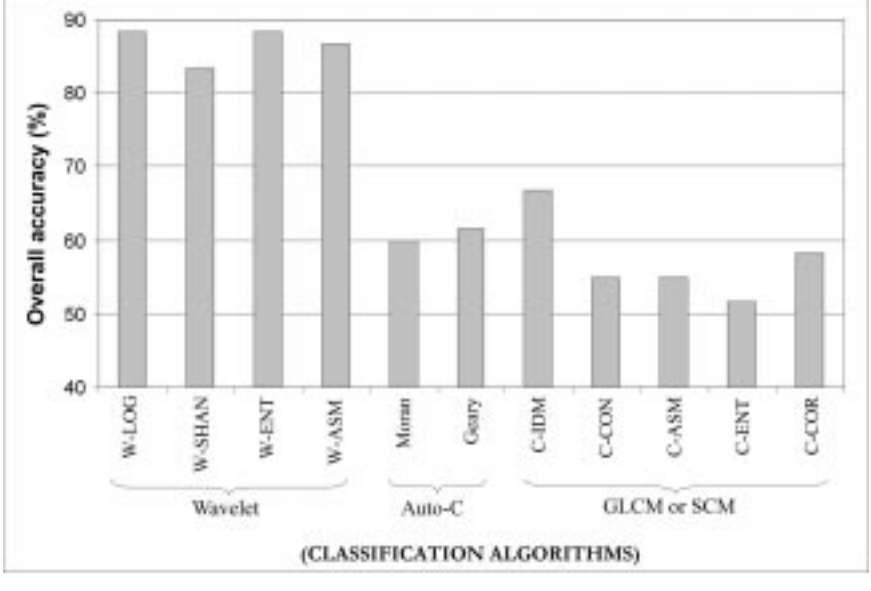

Figure 13 Overall classification accuracies for 33×33 samples generated from band-6 produced by wavelet, spatial autocorrelation, spatial co-occurrence matrix, and fractal analysis approaches

between spatial autocorrelation and the spatial co-occurrence matrix since the C-IDM approach produced better accuracy than both autocorrelation methods, whereas the remainder of the co-occurrence approaches produced lower accuracy than Moran's I and Geary's C. However, it is clear that the accuracies for 33×33 pixel samples

Table 4 Overall classification accuracies for band-6 produced by different algorithms

Overall classification accuracy					
Wavelet		Autocorrelation		Cooccurrence matrix	
W-LOG	88.3	Moran's *I*	60.0	C-IDM	66.7
W-SHAN	83.3	Geary's *C*	61.7	C-CON	55.0
W-ENT	88.3			C-ASM	55.0
W-ASM	86.7			C-ENT	51.7
				C-COR	58.3

achieved by all wavelet transform approaches are much higher than these two texture methods.

8 Conclusions

Figure 10 confirms that the classification accuracy decreases with increasing level of decomposition. It also suggests that the combination of more levels improves the accuracy significantly. When comparing different decomposition approaches, the standard approach was slightly more accurate than the remainder; the vertical decomposition produced slightly higher accuracy than the horizontal decomposition; and the diagonal approach yielded the lowest overall accuracy. However, it should not be interpreted that the overall accuracy obtained by the vertical decomposition would always be higher than that of horizontal accuracy, and vice versa. The spatial dependence of variability in digital values may have a directional component (Lark 1996) such that more variation is seen in one direction than another. The results may vary due to the size of window, choice of the texture measures, type of classes, resolution of the image, nature of textures, selection of wavelet decomposition approach, and type of wavelet transform. These attributes can be considered the sources of error or uncertainty in the application of image texture to urban land cover classification using the wavelet transform approach.

One final result of interest concerns the lack of consistency in overall classification associated with the use of texture measures. Individual performance in the classification varies by the choice of decomposition approach and the use of measures. Hence, it may be difficult to draw a straightforward conclusion on which approach in combination with which texture measure is the most efficient in extracting urban features in this analysis at this point. However, the overall accuracy obtained by the standard decomposition procedure with all four different measures – *LOG*, *SHAN*, *ENT*, and *ASM* – exceeded the minimum mapping accuracy of 85%. Hence, the results from this study suggest that the standard decomposition approach is the most accurate approach in urban texture analysis and classification.

When comparing the wavelet approach with the spatial autocorrelation and spatial co-occurrence approaches, the multi-resolution wavelet approach that combines all three decomposition levels definitely yielded far more accurate results than the other two approaches which do not utilize multi-resolution information. This is an important result. More research on the various aspects of the wavelet approaches

(e.g. different wavelet transform, window size, land-cover classes) will be beneficial to accurate classification of urban features using high-resolution remote sensing imagery.

Acknowledgements

This research was partially supported by grants from the Otis Paul Starkey Fund (The Association of American Geographers) and the Robert C West Field Research Fund (Department of Geography and Anthropology, Louisiana State University). The authors thank DeWitt Braud, Department of Geography and Anthropology, Louisiana State University for providing the ATLAS data used for this study.

References

Albuz E, Kocalar E, and Khokhar A A 1999 Vector-wavelet based scalable indexing and retrieval system for large color image archives. *IEEE Transactions on Geoscience and Remote Sensing* 44: 3021–4

Arai K 1993 A classification method with a spatial-spectral variability. *International Journal of Remote Sensing* 14: 699–709

Avery T E and Berlin G L 1992 *Fundamentals of Remote Sensing and Airphoto Interpretation*. New York, Macmillan

Barber D G and LeDrew E F 1991 SAR Sea Ice Discrimination Using Texture Statistics: A Multivariate Approach. *Photogrammetric Engineering and Remote Sensing* 57: 385–95

Barnsley M J and Barr S L 1996 Inferring Urban Land Use from Satellite Sensor Images Using Kernel-Based Spatial Reclassification. *Photogrammetric Engineering and Remote Sensing* 62: 949–58

Barnsley M J, Barr S L, and Sadler G J 1991 Spatial re-classification of remotely sensed images for urban land-use monitoring In *Proceedings of Spatial Data 2000*, Oxford, 17–20 September, Remote Sensing Society, Nottingham: 106–17

Berry L R and Goutsias J 1991 A comparative study of matrix measures for maximum likelihood texture classification. *IEEE Transactions on Systems, Man, and Cybernetics* 21: 252–61

Brodatz P 1966 *Textures: A Photographic Album for Artists and Designers*. New York, Dover

Burrough P A 1993 Soil Variability: A Late 20th Century View. *Soils and Fertilizers* 56: 529–62

Clarke K C 1986 Computation of the fractal dimension of topographic surfaces using the triangular prism surface area method. *Computers and Geosciences* 12: 713–22

Conners R W and Harlow C 1980 A theoretical comparison of texture algorithms. *IEEE Transactions on Pattern Analysis and Machine Intelligence* 2: 204–22

De Jong S M and Burrough P A 1995 A fractal approach to the classification of Mediterranean vegetation types in remotely sensed images. *Photogrammetric Engineering and Remote Sensing* 61: 1041–53

Dong P 2000a Lacunarity for spatial heterogeneity measurement in GIS. *Geographic Information Sciences* 6: 20–6

Dong P 2000b Test of a new lacunarity estimation method for image texture analysis. *International Journal of Remote Sensing* 17: 3369–73

Emerson C W, Lam N S N, and Quattrochi D A 1999 Multi-scale fractal analysis of image texture and pattern. *Photogrammetric Engineering and Remote Sensing* 65: 51–61

Edwards G, Landary R, and Thomson K P B 1988 Texture analysis of forest regeneration sites in high-resolution SAR imagery. In *Proceedings of the International Geosciences and Remote Sensing Symposium* (IGARSS 88). Paris, European Space Agency Report No SP 284: 1355–60

Fortin M J 1992 Detection of Ecotones: Definition and Scaling Factors. Unpublished PhD Dissertation, State University of New York at Buffalo

Foster B C 1985 An examination of some problems and solutions in monitoring urban areas from satellite platforms. *International Journal of Remote Sensing* 6: 139–51

Fukuda S and Hirosawa H 1998 Suppression of speckle in synthetic aperture radar images using wavelet. *International Journal of Remote Sensing* 19: 507–19

Gong P and Howarth P J 1990 The use of structural information for improving land cover classification accuracies at the rural urban fringe. *Photogrammetric Engineering and Remote Sensing* 56: 67–73

Gong P and Howarth P J 1992 Frequency based contextual classification and gray level vector reduction for land use identification. *Photogrammetric Engineering and Remote Sensing* 58: 423–37

Green D R, Cummins R, Wright R, and Miles J 1993 A methodology for acquiring information on vegetation succession from remotely sensed imagery. In Haines-Young R, Green D R, and Cousins S (eds) *Landscape Ecology and Geographic Information Systems*. London, Taylor and Francis: 111–28

Haack B, Bryant N, and Adams S 1987 An assessment of Landsat MSS and TM data for urban and near-urban land-cover digital classification. *Remote Sensing of Environment* 21: 201–13

Haralick R M, Shanmugan K, and Dinstein J 1973 Textural features for image classification. *IEEE Transaction on Systems, Man, and Cybernetics* 3: 610–21

Hodgson M E 1998 What size window for image classification? A cognitive perspective. *Photogrammetric Engineering and Remote Sensing* 64: 797–807

Ji M and Jensen J R 1999 Effectiveness of subpixel analysis in detecting and quantifying urban imperviousness from Landsat Thematic Mapper imagery. *Geocarto International* 14: 33–48

Klinkenberg B 1992 Fractals and morphometric measures: Is there a relationship? *Geomorphology* 5: 5–20

Klinkenberg B and Goodchild M F 1992 The fractal properties of topography: A comparison of methods. *Earth Surface Processes and Landforms* 17: 217–34

Lam N S N 1990 Description and measurement of Landsat TM images using fractals. *Photogrammetric Engineering and Remote Sensing* 56: 187–95

Lam N S N and De Cola L 1993 Fractal simulation and interpolation. In Lam N S N and De Cola L (eds) *Fractals in Geography*. Englewood Cliffs, NJ, Prentice Hall: 56–74

Lam N S N and Quattrochi D A 1992 On the issues of scale, resolution, and fractal analysis in the mapping sciences. *Professional Geographer* 44: 88–97

Lam N S N, Quattrochi D, Qui H, and Zhao H 1998 Environmental assessment and monitoring with image characterization and modeling system using multiscale remote sensing data. *Applied Geographic Studies* 2: 77–93

Lam N S N, Qui H, Quattrochi D A, and Emerson C W 2002 An evaluation of fractal methods for characterizing image complexity. *Cartography and Geographic Information Science* 29: 25–35

Lark R M 1996 Geostatistical description of texture on an aerial photograph for discriminating classes of land cover. *International Journal of Remote Sensing* 17: 2115–33

Mallat S G 1989a A Theory for multi-resolution signal decomposition: The wavelet representation. *IEEE Transactions on Pattern Analysis and Machine Intelligence* 11: 674–93

Mallat S G 1989b Multifrequency channel decompositions of images and wavelet representation. *IEEE Transactions on Acoustics, Speech, and Signal Processing* 37: 2091–110

Mark D M and Aronson P B 1984 Scale dependent fractal dimensions of topographic surfaces: An empirical investigation with applications in geomorphology and computer mapping. *Mathematical Geology* 16: 671–83

Martin L R G, Howarth P G, and Holder G 1988 Multispectral classification of land use at the rural-urban fringe using SPOT data. *Canadian Journal of Remote Sensing* 14: 72–9

Metzger J P and Muller E 1996 Characterizing the complexity of landscape boundaries by remote sensing. *Landscape Ecology* 11: 65–77

Muller E 1997 Mapping riparian vegetation along rivers: Old concepts and new methods. *Aquatic Botany* 58: 411–37

Myint S W 2001 Wavelet Analysis and Classification of Urban Environment Using High-resolution Multispectral Image Data. Unpublished PhD Dissertation, Louisiana State University

Myint S W 2002 A robust texture analysis and classification approach for urban land use and land cover feature discrimination. *GeoCarto International* 16: 27–38

Peddle D R and Franklin S E 1991 Image texture processing and data integration for surface

pattern discrimination. *Photogrammetric Engineering and Remote Sensing* 57: 413–20
Pesaresi M 2000 Texture analysis for urban pattern recognition using fine-resolution panchromatic satellite imagery. *Geographical and Environmental Modeling* 4: 43–63
Quattrochi D A, Lam N S N, Qiu H, and Zhao W 1997 Image Characterization and Modeling System (ICAMS): A geographic information system for the characterization and modeling of multiscale remote sensing data. In Quattrochi D A and Goodchild M F (eds) *Scale in Remote Sensing and GIS*. Boca Raton, FL, CRC Press: 295–308
Roach D and Fung K B 1994 Fractal-based textural descriptors for remotely sensed forestry data. *Canadian Journal of Remote Sensing* 20: 59–70
Sadler G J, Barnsley M J, and Barr S L 1991 Information extraction from remotely-sensed images for urban land analysis. In *Proceedings of the Second European Conference on Geographical Information Systems (EGIS'91)*. Utrecht, EGIS Foundation: 955–64
Sheikholeslami G, Zhang A, and Bian L 1999 A multi-resolution content-based retrieval approach for geographic images. *Geoinformatica* 3: 109–39
Snow R S and Mayer L 1992 Fractals in geomorphology. *Geomorphology* 5: 19–24
Strang G and Nguyen T 1997 *Wavelets and Filter Banks*. Wellesley, MA, Wellesley-Cambridge Press
Townshend J R G 1981 *Terrain Analysis and Remote Sensing*. London, George Allen and Unwin
Webster R, Curran P J, and Munden J W 1989 Spatial correlation in reflected radiation from the ground and its implication for sampling and mapping by ground-based radiometry. *Remote Sensing of Environment* 29: 67–78
Woodcock C E, Strahler A H, and Jupp D L B 1988a The use of variograms in remote sensing: Part 1, Scene models and simulated images. *Remote Sensing of Environment* 25: 323–48
Woodcock C E, Strahler A H, and Jupp D L B 1988b The use of variograms in remote sensing: Part 2, Real digital images. *Remote Sensing of Environment* 25: 323–48
Woodcock C and Harward V J 1992 Nested-hierarchical scene models and image segmentation. *International Journal of Remote Sensing* 13: 3167–87
Xia Z 1993 The Uses and Limitations of Fractal Geometry in Digital Terrain Modeling. Unpublished PhD Dissertation, City University of New York
Zhu C and Yang X 1998 Study of remote sensing image texture analysis and classification using wavelet. *International Journal of Remote Sensing* 13: 3167–87